Supporting information of **"Evaluating the use of smart sensors in ground-based monitoring of landslide movement with laboratory experiments"**

Alessandro Sgarabotto[1], Irene Manzella[1,2], Kyle Roskilly[3], Miles J. Clark[4], Georgie L. Bennett[5], Chunbo Luo[6], Aldina M. A. Franco[4]

[1]School of Geography, Earth and Environmental Sciences, University of Plymouth, Plymouth, UK
[2]Faculty of Geo-Information Science and Earth Observation, University of Twente, Enschede, NL
[3]Environment and Sustainability Institute, University of Exeter, Penryn, UK
[4]School of Environmental Sciences, University of East Anglia, Norwich, UK
[5]Department of Geography, University of Exeter, Exeter, UK
[6]Department of Computer Science, University of Exeter, Exeter, UK

Correspondence to: Alessandro Sgarabotto (alessandro.sgarabotto@plymouth.ac.uk)

1 Methods

1.1 Sensor calibration

The measurement model for an accelerometer reads as (Frosio et al., 2009)

$$\boldsymbol{a}_g = M(\boldsymbol{a} - \boldsymbol{b}_a) \quad (1)$$

where $\boldsymbol{a}_g$ is the calibrated acceleration in unit of g, M is the error matrix, $\boldsymbol{a}$ is the acceleration after the offset and $\boldsymbol{b}_a$ is the bias. In the error matrix M, diagonal elements are the scale factors along the three axes, whereas the extra diagonal elements are due to both axes misalignment and crosstalk effects. Assuming M symmetrical, there are 8 unknown parameters in eq. (1), e.g. 5 unknowns in M and 3 unknowns in $\boldsymbol{b}_a$. These parameters are computed through a nonlinear optimization so that, in static conditions, the intensity of the acceleration vector equals the g acceleration. Collecting data in N random static positions (N>30), a least squares method allows computing the unknown parameters Frosio et al. (2008). The acceleration data used for the calibration procedure are represented in Figure S1.

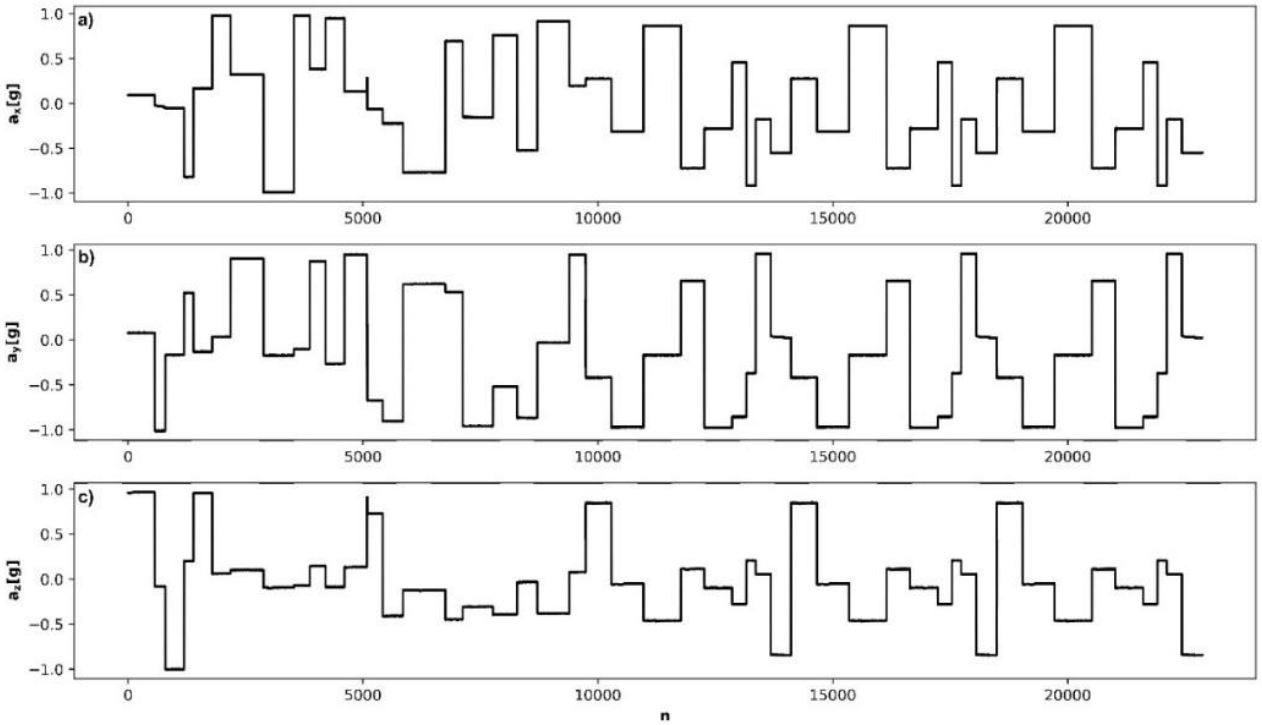

Figure S1. Raw acceleration recordings in static positions used for accelerometers calibration.

Under steady conditions, the angular velocity is expected to be nil. Thus, each of the three axes of the gyro should read 0 ˚/s when the gyroscope is in a still position. For this reason, the simplest calibration of a gyroscope consists of calculating the offset for each axis. The offsets are measured by record the signal when gyroscope is in a static position and then averaging the signal recorded in each direction. Without considering additional noise sources, the measurement error model for a gyroscope applied in all three directions read as (Glueck et al., 2013)

$$\dot{\boldsymbol{\varphi}} = \dot{\boldsymbol{\varphi}}_m - \dot{\boldsymbol{\varphi}}_O \tag{2}$$

where $\dot{\boldsymbol{\varphi}}$ is the calibrated angular velocity, $\dot{\boldsymbol{\varphi}}_m$ is the gyro reading, $\dot{\boldsymbol{\varphi}}_O$ is the gyroscope offset. The gyroscope data used for the calibration procedure are represented in Figure S2.

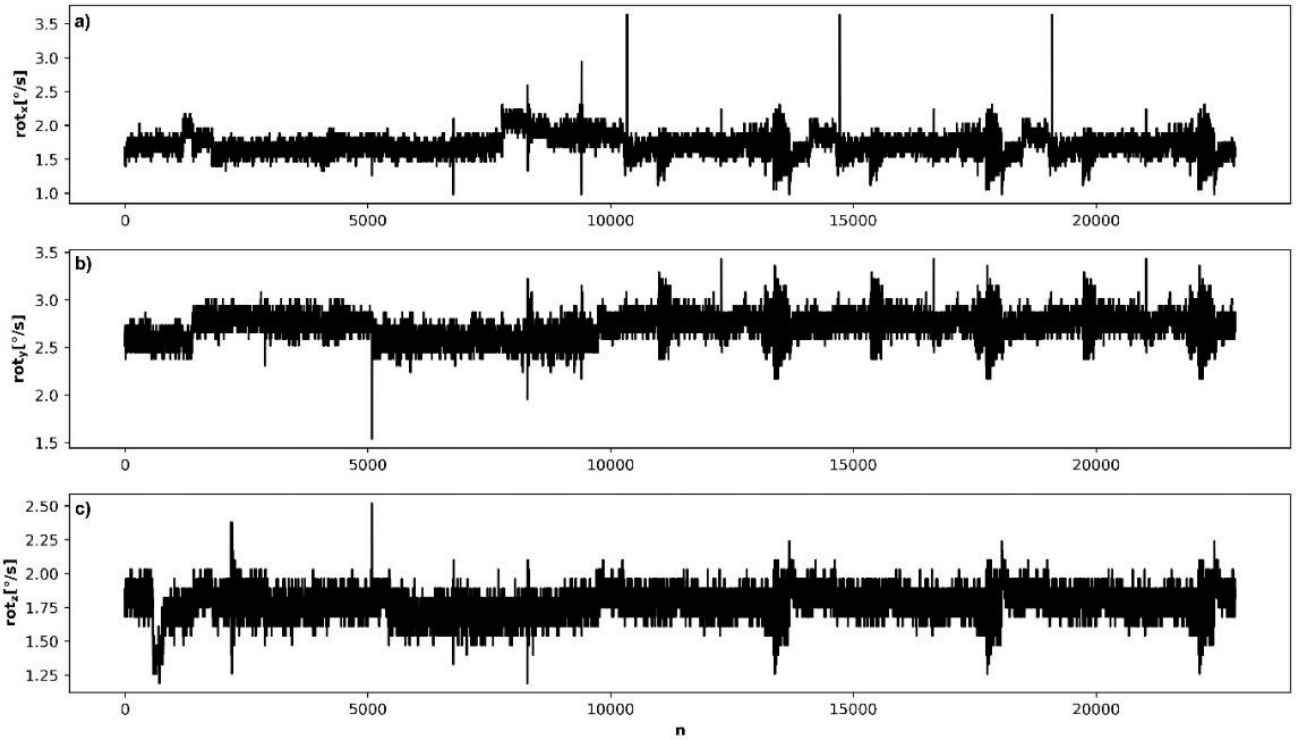

Figure S2. Raw angular velocity recordings in static positions used for gyroscopes calibration.

The measurement error for a magnetometer read as (Dewhirst et al., 2016)

$$\boldsymbol{mag}_m = S\mathcal{N}(A_{si}\,\boldsymbol{mag} - \boldsymbol{b}_{hi}) + \boldsymbol{b}_m \quad (3)$$

where $\boldsymbol{mag_m}$ is the magnetic field measured by sensors, S is scale factor to generate outputs that fall within our desired range, $\mathcal{N}$ is the misalignment error, $\boldsymbol{b}_m$ is the bias error (offset), $\boldsymbol{b}_{hi}$ is hard iron errors due to the presence of permanent magnets and residual magnetism, A_{si} is soft iron errors due to presence of material that influences or distorts a magnetic field, but does not necessarily generate a magnetic field itself and $\boldsymbol{mag}$ is the actual magnetic field. Hence, the calibrated magnetic field can be computed as

$$\boldsymbol{mag} = A_m^{-1}\left(\boldsymbol{mag}_m - \overline{\boldsymbol{b}}\right) \quad (4)$$

where $A_m = S\mathcal{N}A_{si}$ and $\overline{\boldsymbol{b}} = S\mathcal{N}\boldsymbol{b}_{hi} + \boldsymbol{b}_m$. The calibration procedure aims at taking the points over an elliptic surface, finding the offset, and recasting them over a spherical surface. The calibration procedure computes the arrays A_m^{-1} and $\overline{\boldsymbol{b}}$ by using the orthogonality property of the magnetic field vector (Dewhirst et al., 2016). The magnetometer data used for the calibration procedure are represented in Figure S3.

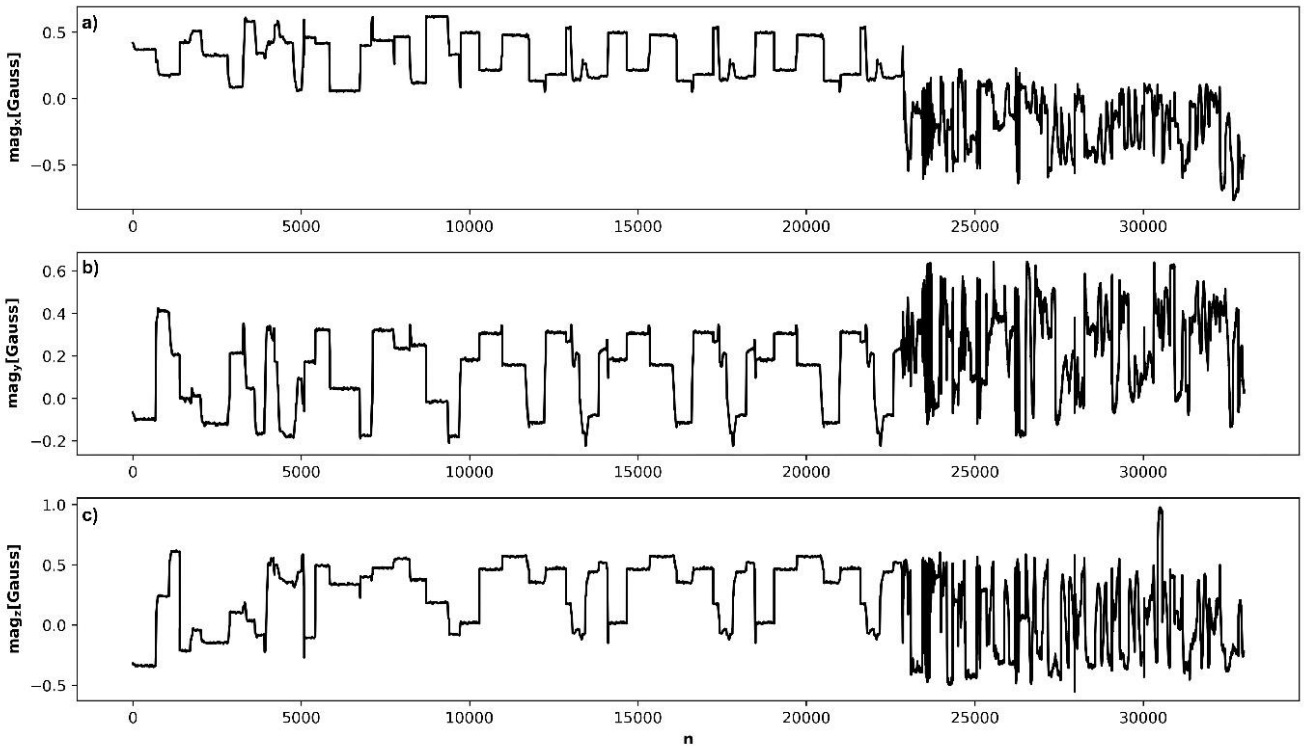

Figure S3. Raw magnetometer recordings used for magnetometers calibration.

1.2 Kalman filter

The Kalman filter is a recursive algorithm that provides an estimate of the state of the system given some measurements. The unknown variables are usually noisy and define the state of the system $\boldsymbol{x}$. Conversely, the measurements $\boldsymbol{z}$ are reliable temporal observations feeding the algorithm to improve the estimate of the state of the system (Dewhirst et al., 2016; Kim and Bang, 2019). The model describes the evolution of the state from k to $k-1$ as (Kim and Bang, 2019)

$$\boldsymbol{x}_k = A\boldsymbol{x}_{k-1} + B\boldsymbol{u}_{k-1} + \boldsymbol{w}_{k-1} \quad (1)$$

where A is the transition matrix applied to the previous state $k-1$, B is the control-input matrix applied to the control vector $\boldsymbol{u}_{k-1}$ and $\boldsymbol{w}_{k-1}$ is the process noise vector. In the Kalman filter process model, the noise is assumed to be a zero-mean Gaussian variable with Q as covariance, i.e. $\boldsymbol{w} \approx \mathcal{N}(0, Q)$. In the present application, the state of the system at the step k is defined as

$$\boldsymbol{x}_k = [x, y, z, v_x, v_y, v_z, a_x, a_y, a_z]^T \quad (2)$$

where x, y, z are the position components, v_x, v_y, v_z are the velocity components and a_x, a_y, a_z are the acceleration components. The transition matrix A and the control-input matrix B are defined as

$$A = \begin{bmatrix} 1 & 0 & 0 & \Delta t & 0 & 0 & 1/2\Delta t^2 & 0 & 0 \\ 0 & 1 & 0 & 0 & \Delta t & 0 & 0 & 1/2\Delta t^2 & 0 \\ 0 & 0 & 1 & 0 & 0 & \Delta t & 0 & 0 & 1/2\Delta t^2 \\ 0 & 0 & 0 & 1 & 0 & 0 & \Delta t & 0 & 0 \\ 0 & 0 & 0 & 0 & 1 & 0 & 0 & \Delta t & 0 \\ 0 & 0 & 0 & 0 & 0 & 1 & 0 & 0 & \Delta t \\ 0 & 0 & 0 & 0 & 0 & 0 & 1 & 0 & 0 \\ 0 & 0 & 0 & 0 & 0 & 0 & 0 & 1 & 0 \\ 0 & 0 & 0 & 0 & 0 & 0 & 0 & 0 & 1 \end{bmatrix} ; \qquad B = [0]_{9x6} \qquad (3)$$

where Δt is the time step, that in the present application is equal to 0.017 s. The state-evolution equation is coupled with the measurement model describing the relation between the measurement $\boldsymbol{z}_k$ and the state $\boldsymbol{x}_k$ (Kim and Bang, 2019)

$$\boldsymbol{z}_k = H\boldsymbol{x}_k + \boldsymbol{\nu}_{k-1} \qquad (4)$$

where H is the measurement matrix and $\boldsymbol{\nu}_k$ the noise of the measurements assumed to be a zero-mean gaussian variable with R as covariance, i.e. $\boldsymbol{\nu} \approx \mathcal{N}(0, P)$. In the present application, the measurement vector $\boldsymbol{z}$ stores the camera-based positions x_m, y_m, z_m and the IMU-based linear accelerations $a_{x,m}$, $a_{y,m}$, $a_{z,m}$ and at the step k reads as

$$\boldsymbol{z}_k = [x_m, y_m, z_m, 0,0,0, a_{x,m}, a_{y,m}, a_{z,m}]^T \qquad (5)$$

The measurement matrix H is defined as:

$$H = \begin{bmatrix} 1 & 0 & 0 & 0 & 0 & 0 & 0 & 0 & 0 \\ 0 & 1 & 0 & 0 & 0 & 0 & 0 & 0 & 0 \\ 0 & 0 & 1 & 0 & 0 & 0 & 0 & 0 & 0 \\ 0 & 0 & 0 & 0 & 0 & 0 & 1 & 0 & 0 \\ 0 & 0 & 0 & 0 & 0 & 0 & 0 & 1 & 0 \\ 0 & 0 & 0 & 0 & 0 & 0 & 0 & 0 & 1 \end{bmatrix} \qquad (6)$$

The Kalman filter algorithm consists of two stages, prediction, and update. The state is predicted from a former state and then is updated using the measurements available for the process investigated. The iterative process starts from the initial uncertainty regarding the state and the measurements. The initial measurement noise is 10-14 m for position and 10-8 m/s2 for acceleration in the case of rolling experiments and 10-6 m/s2 in the case of sliding experiments.

2 Additional results

2.1 Cobble experiments

Additional comparisons between the modelling framework and the filtered data are shown in Figure S4-S17.

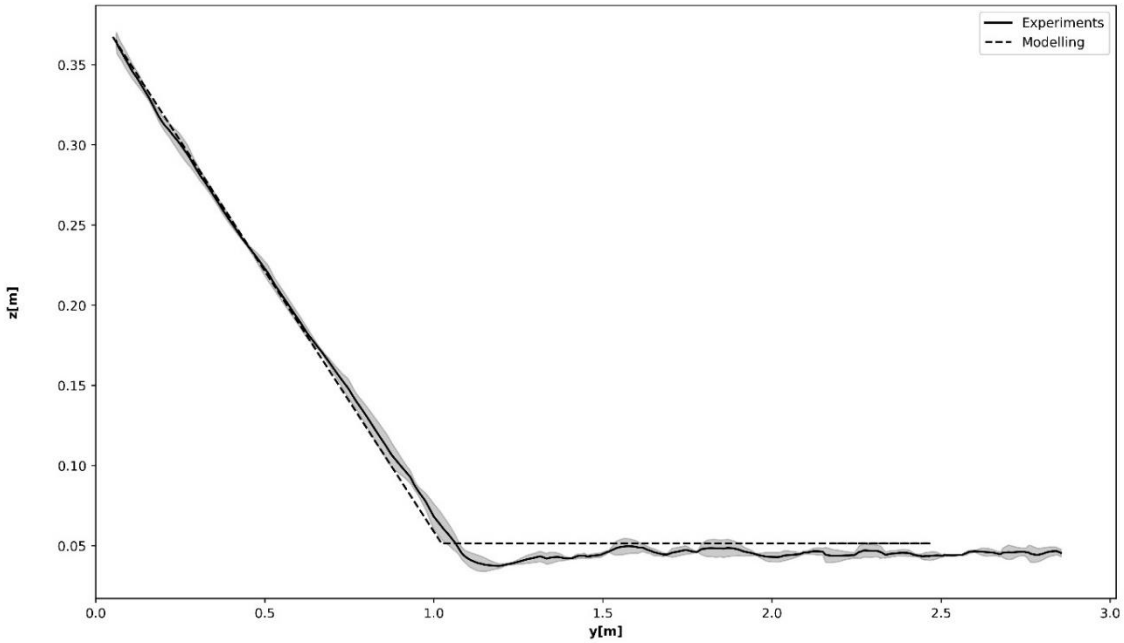

Figure S4. Comparison between the experiments and the analytical model describing the trajectories of the cobble on a 18° incline in the vertical plane z-y. The response of the conceptual model is obtained for r =0 m and Φ = 7.5°. Solid lines represent the average behaviour during the experiments at the same slope, whereas the grey area show the standard deviation of the variable considered.

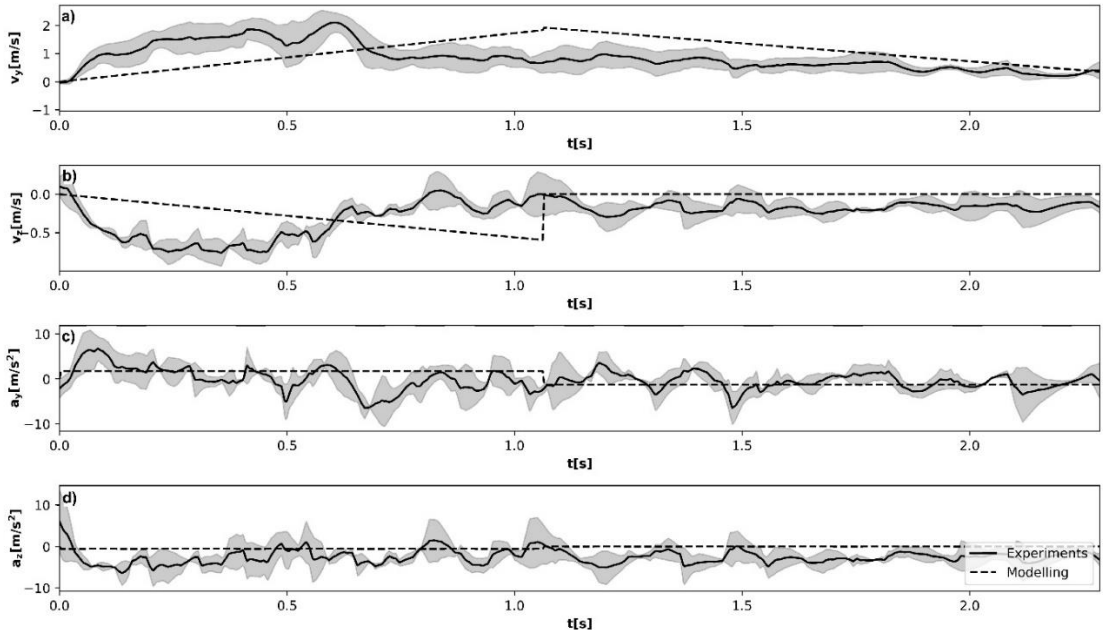

Figure S5. Comparison between the experimental results and the analytical model for rolling experiments on a 18° incline. (a) Horizontal velocity v_y. (b) Vertical velocity v_z. (c) Horizontal acceleration a_y. (d) Vertical acceleration a_z. Dashed lines show the response of the conceptual model obtained r =0 m and Φ = 7.5° for the sliding experiments. Solid lines represent the average behaviour during the experiments at the same slope, whereas the grey area show the standard deviation of the variable considered.

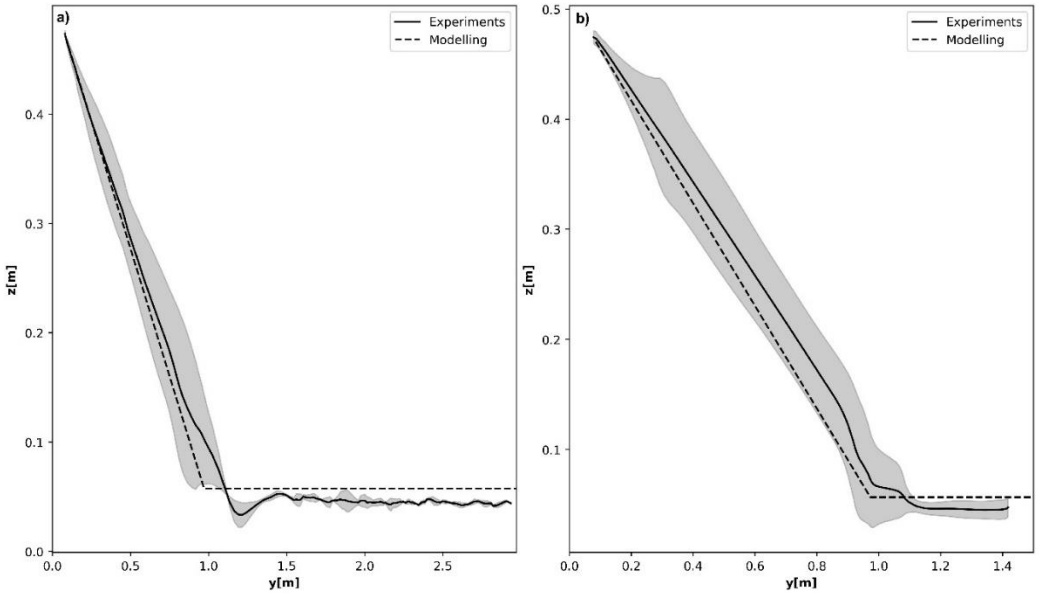

Figure S6. Comparison between the experiments and the analytical model describing the trajectories of the cobble on a 25° incline in the vertical plane z-y. (a) Rolling experiments where the response of the conceptual model is obtained for r =0 m and Φ = 7.5°. (b) Sliding experiments where the response of the conceptual model is obtained for r =0 m and Φ = 2.5 °. Solid lines represent the average behaviour during the experiments at the same slope, whereas the grey area show the standard deviation of the variable considered.

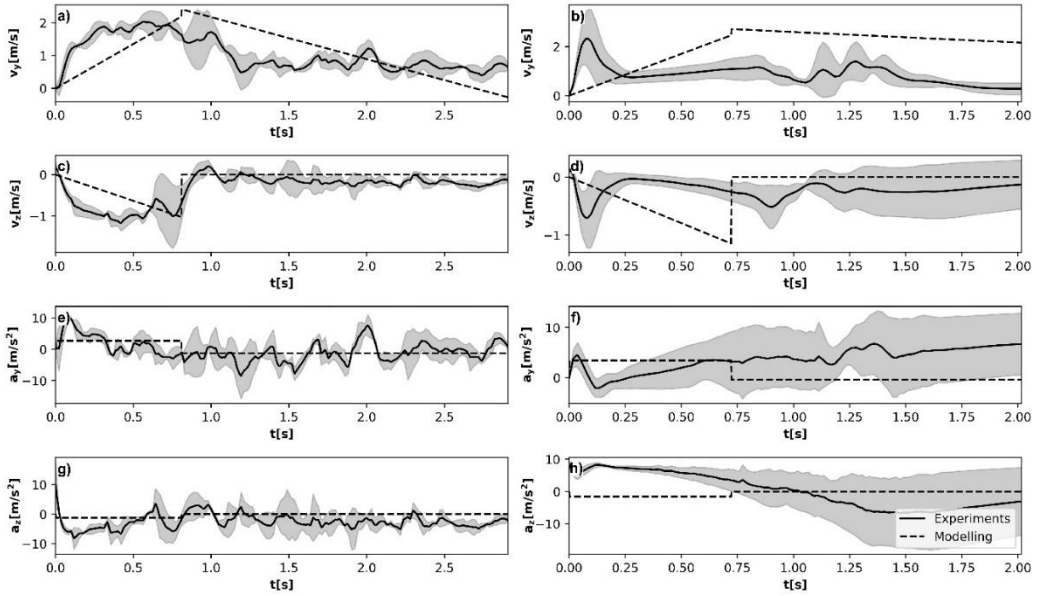

Figure S7. Comparison between the experimental results and the analytical model for (a, c, e, and g) rolling and (b, d, f, and h) sliding on a 25° incline. (a and b) Horizontal velocity v_y. (c and d) Vertical velocity v_z. (e and f) Horizontal acceleration a_y. (g and h) Vertical acceleration a_z. Dashed lines show the response of the conceptual model obtained r =0 m and Φ = 7.5° for the sliding

experiments and r =0 and Φ =2.5° for the sliding experiments. Solid lines represent the average behaviour during the experiments at the same slope, whereas the grey area shows the standard deviation of the variable considered.

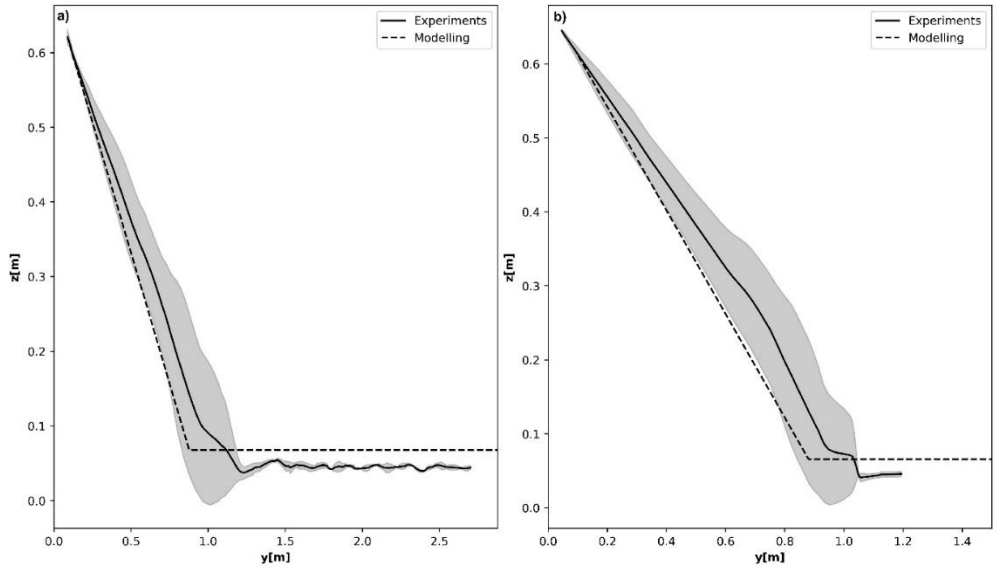

Figure S8. Comparison between the experiments and the analytical model describing the trajectories of the cobble on a 35° incline in the vertical plane z-y. (a) Rolling experiments where the response of the conceptual model is obtained for r =0 m and Φ = 7.5°. (b) Sliding experiments where the response of the conceptual model is obtained for r =0 m and Φ = 2.5°. Solid lines represent the average behaviour during the experiments at the same slope, whereas the grey area show the standard deviation of the variable considered.

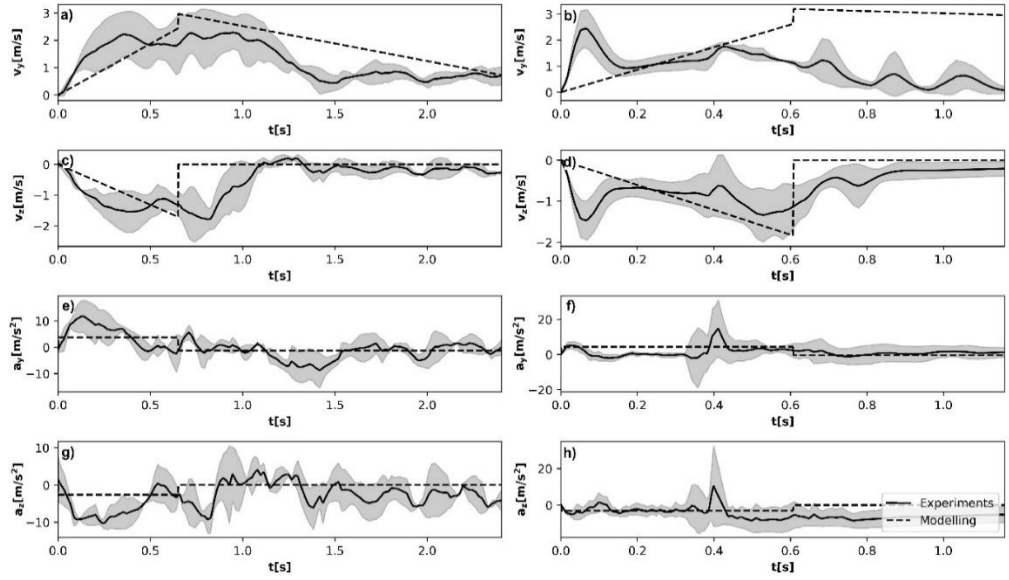

Figure S9. Comparison between the experimental results and the analytical model for (a, c, e, and g) rolling and (b, d, f, and h) sliding on a 35° incline. (a and b) Horizontal velocity v_y. (c and d) Vertical velocity v_z. (e and f) Horizontal acceleration a_y. (g and h) Vertical acceleration a_z. Dashed lines show the response of the conceptual model obtained r =0 m and Φ = 7.5° for the sliding

experiments and r =0 and Φ =2.5° for the sliding experiments. Solid lines represent the average behaviour during the experiments at the same slope, whereas the grey area shows the standard deviation of the variable considered.

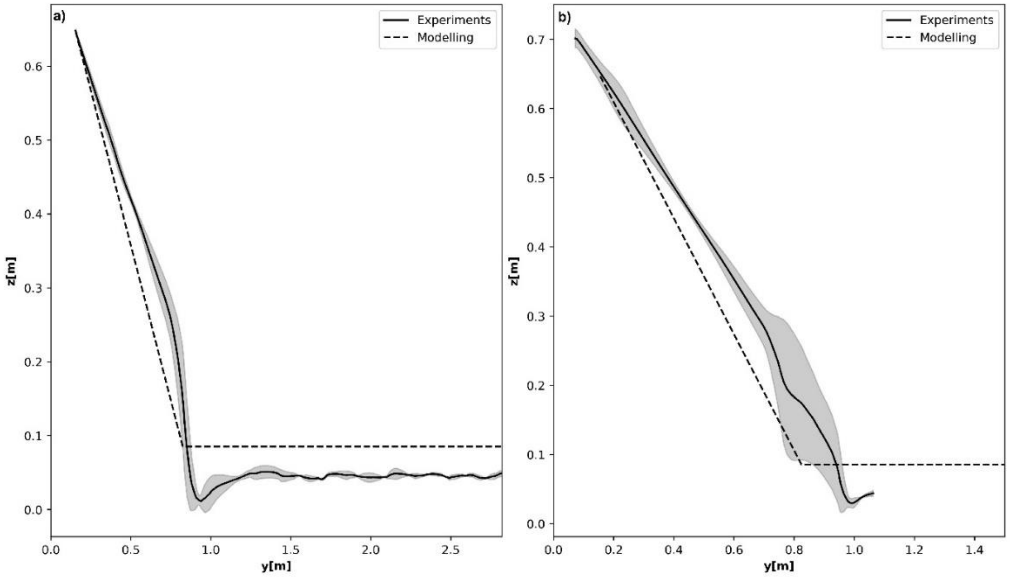

Figure S10. Comparison between the experiments and the analytical model describing the trajectories of the cobble on a 40° incline in the vertical plane z-y. (a) Rolling experiments where the response of the conceptual model is obtained for r =0 m and Φ = 7.5°. (b) Sliding experiments where the response of the conceptual model is obtained for r =0 m and Φ = 2.5°. Solid lines represent the average behaviour during the experiments at the same slope, whereas the grey area show the standard deviation of the variable considered.

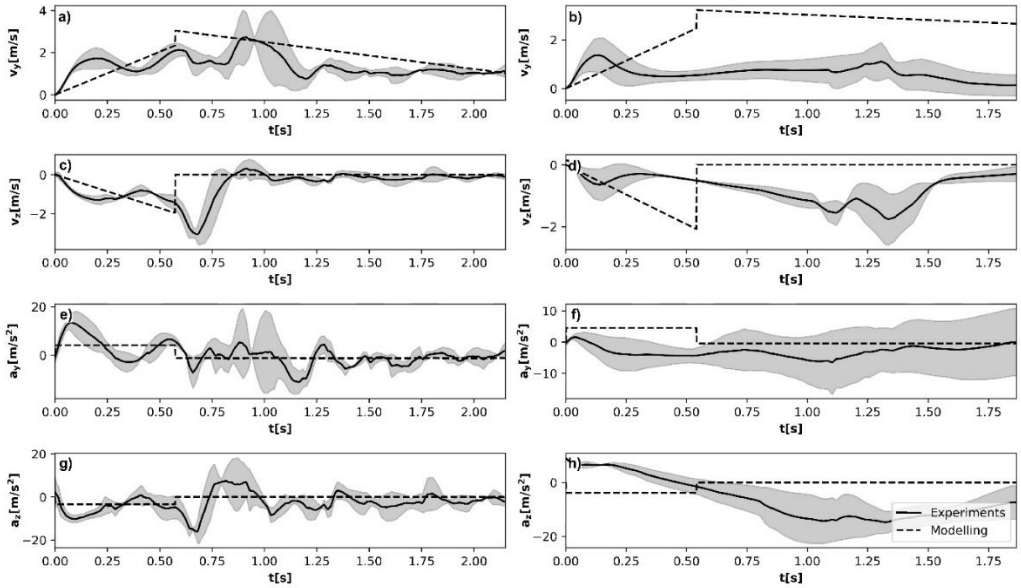

Figure S11. Comparison between the experimental results and the analytical model for (a, c, e, and g) rolling and (b, d, f, and h) sliding on a 40° incline. (a and b) Horizontal velocity v_y. (c and d) Vertical velocity v_z. (e and f) Horizontal acceleration a_y. (g and h) Vertical acceleration a_z. Dashed lines show the response of the conceptual model obtained r =0 m and Φ = 7.5° for the sliding

experiments and r =0 and Φ =2.5° for the sliding experiments. Solid lines represent the average behaviour during the experiments at the same slope, whereas the grey area shows the standard deviation of the variable considered.

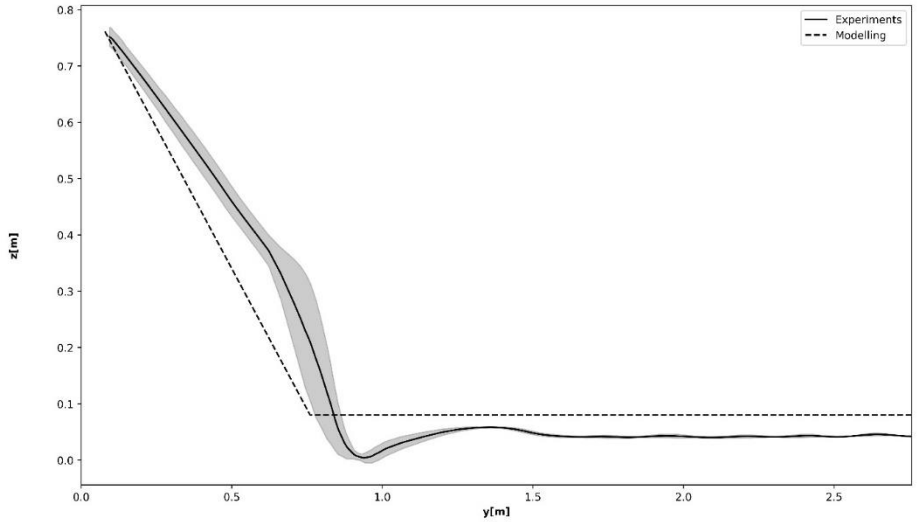

Figure S12. Comparison between the experiments and the analytical model describing the trajectories of the cobble on a 45° incline in the vertical plane z-y. The response of the conceptual model is obtained for r =0 m and Φ = 7.5°. Solid lines represent the average behaviour during the experiments at the same slope, whereas the grey area show the standard deviation of the variable considered.

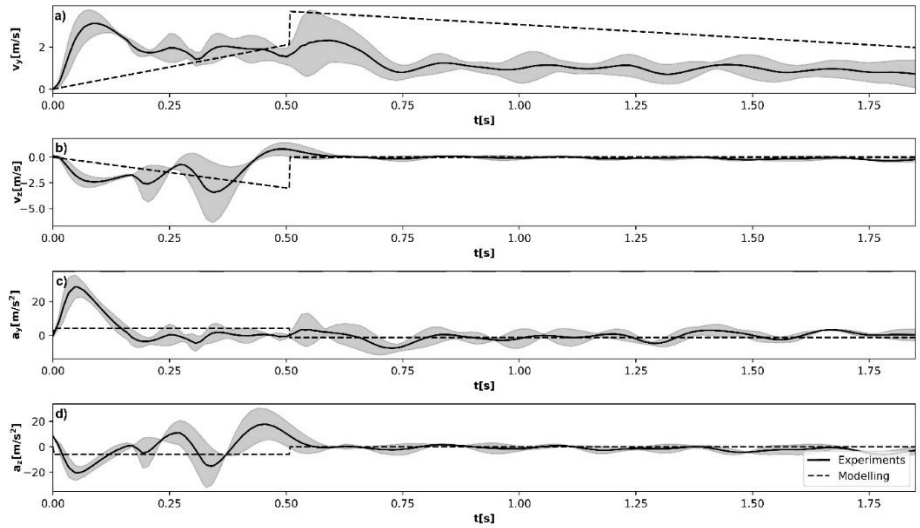

Figure S13. Comparison between the experimental results and the analytical model for rolling experiments on a 45° incline. (a) Horizontal velocity v_y. (b) Vertical velocity v_z. (c) Horizontal acceleration a_y. (d) Vertical acceleration a_z. Dashed lines show the response of the conceptual model obtained r =0 m and Φ = 7.5° for the sliding experiments. Solid lines represent the average behaviour during the experiments at the same slope, whereas the grey area shows the standard deviation of the variable considered.

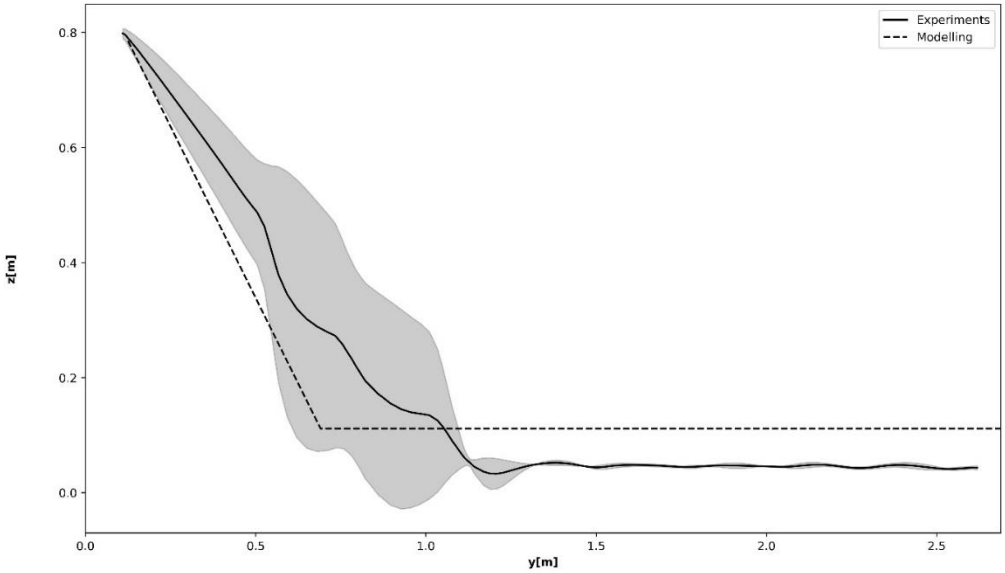

Figure S14. Comparison between the experiments and the analytical model describing the trajectories of the cobble on a 50° incline in the vertical plane z-y. The response of the conceptual model is obtained for r =0 m and Φ = 7.5°. Solid lines represent the average behaviour during the experiments at the same slope, whereas the grey area show the standard deviation of the variable considered.

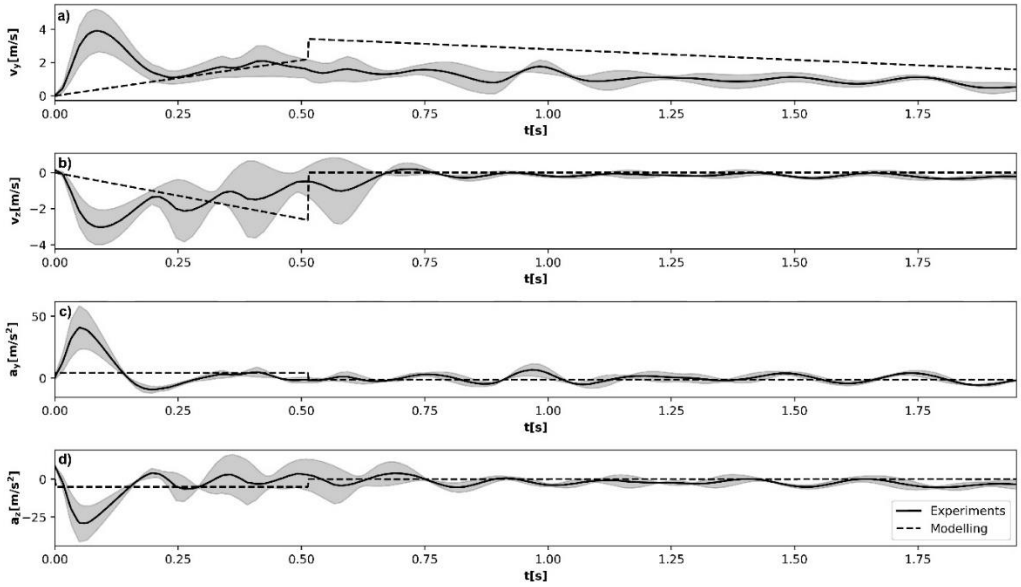

Figure S15. Comparison between the experimental results and the analytical model for rolling experiments on a 50° incline. (a) Horizontal velocity v_y. (b) Vertical velocity v_z. (c) Horizontal acceleration a_y. (d) Vertical acceleration a_z. Dashed lines show the response of the conceptual model obtained r =0 m and Φ = 7.5° for the sliding experiments. Solid lines represent the average behaviour during the experiments at the same slope, whereas the grey area shows the standard deviation of the variable considered.

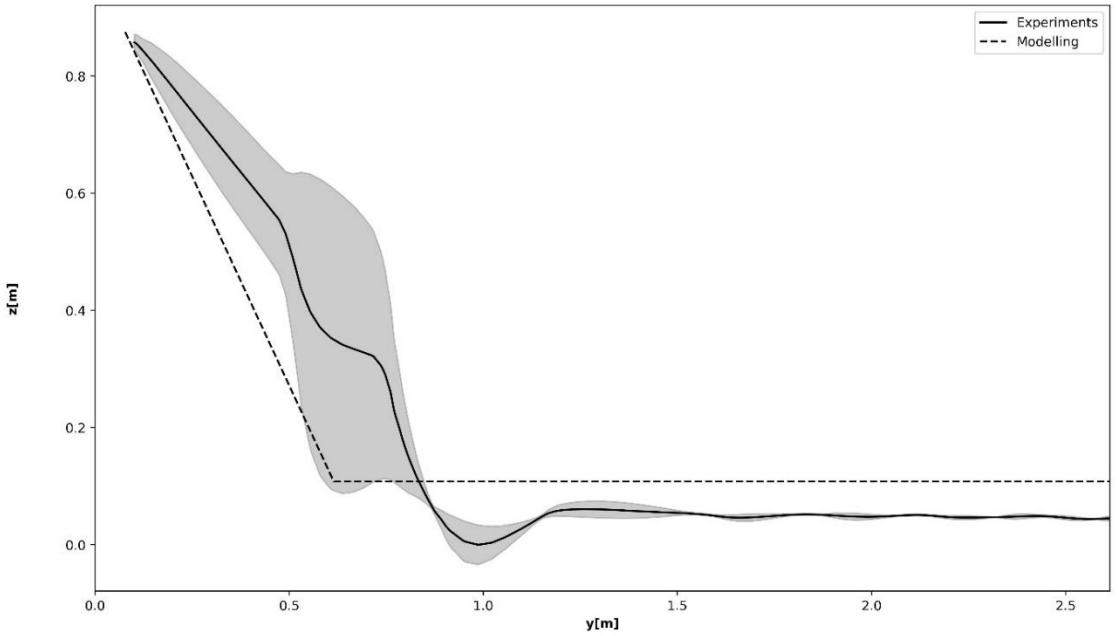

Figure S16. Comparison between the experiments and the analytical model describing the trajectories of the cobble on a 55° incline in the vertical plane z-y. The response of the conceptual model is obtained for r =0 m and Φ = 7.5°.

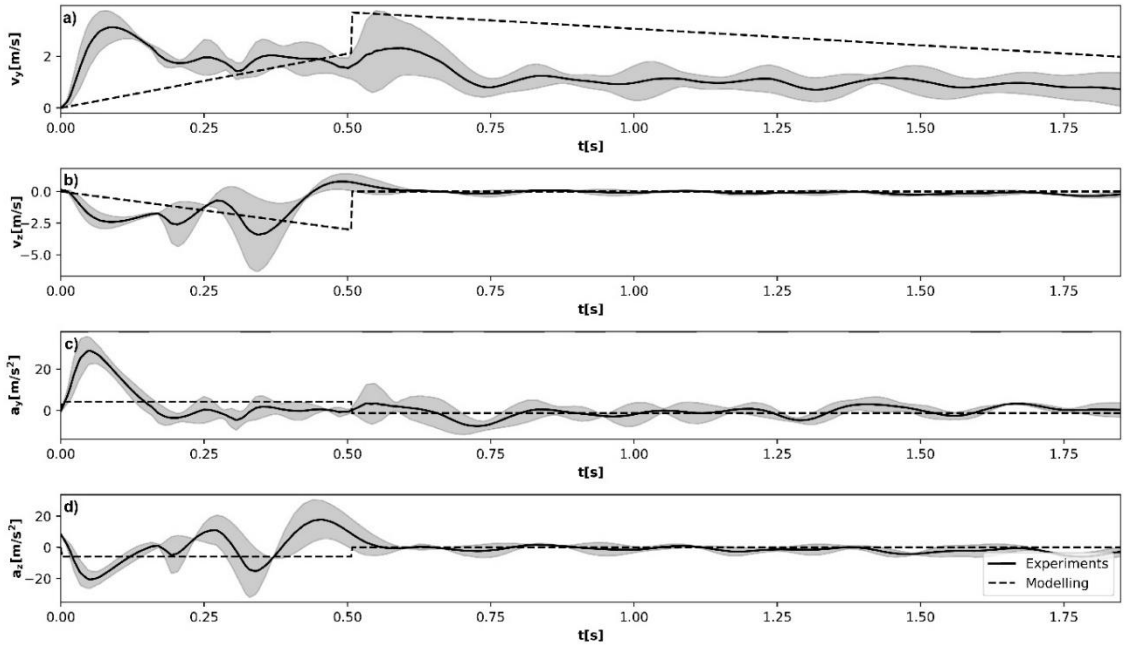

Figure S17. Comparison between the experimental results and the analytical model for rolling experiments on a 55° incline. (a) Horizontal velocity v_y. (b) Vertical velocity v_z. (c) Horizontal acceleration a_y. (d) Vertical acceleration a_z. Dashed lines show the response of the conceptual model obtained r =0 m and Φ = 7.5° for the sliding experiments. Solid lines represent the average behaviour during the experiments at the same slope, whereas the grey area show the standard deviation of the variable considered.

References

Dewhirst, O. P., Evans, H. K., Roskilly, K., Harvey, R. J., Hubel, T. Y. and Wilson, A. M. (2016). Improving the accuracy of estimates of animal path and travel distance using GPS drift-corrected dead reckoning. Ecology and Evolution, 6, 17, 6210-6222. https://doi.org/10.1002/ece3.2359

Frosio, I., Pedersini, F. and Borghese, N. A. (2009). Autocalibration of MEMS accelerometers. IEEE Transactions on Instrumentation and Measurement, 58, 6, 2034-2041, https://10.1109/TIM.2008.2006137.

Glueck, M., Oshinubi, D. and Manoli, Y. (2013) Automatic realtime offset calibration of gyroscopes, 2013 IEEE Sensors Applications Symposium Proceedings, Galveston, TX, USA, 214-218. https://doi.org/10.1109/SAS.2013.6493589

Kim, Y. and Bang, H. (2019). Introduction to kalman filter and its applications. In: F. Govaers, editor, Kalman Filter, chapter 2, 1-17. InTechOpen. https://doi.org/10.5772/intechopen.80600